nature neuroscience

Synchrony-dependent propagation of firing rate in iteratively constructed networks *in vitro*

Alex D Reyes

The precise role of synchronous neuronal firing in signal encoding remains unclear. To examine what kinds of signals can be carried by synchrony, I reproduced a multilayer feedforward network of neurons in an *in vitro* slice preparation of rat cortex using an iterative procedure. When constant and time-varying frequency signals were delivered to the network, the firing of neurons in successive layers became progressively more synchronous. Notably, synchrony in the *in vitro* network developed even with uncorrelated input, persisted under a wide range of physiological conditions and was crucial for the stable propagation of rate signals. The firing rate was represented by a classical rate code in the initial layers, but switched to a synchrony-based code in the deeper layers.

There has been some debate regarding the role of synchrony in nervous system signaling[1–9]. One view is that synchrony is involved in transmitting temporally precise signals. Under this coding scheme, the activities of neurons become correlated during a task or during sensory stimulation[10–23]. Another view is that signals are propagated by a rate code such that the number, and not the timing, of action potentials (APs) is the important variable[2,4,24–26]. In this view, synchrony has only a minor role in, and may even compromise, rate coding[4,26,27].

Detailed analyses of signal propagation have thus far been limited to models of feedforward networks[4,20–23,25–27]. Simulations indicate that depending on the condition, the network can provide a substrate for either a temporal or rate code. In a network of integrate-and-fire neurons, a packet of synchronized APs delivered to the first layer will propagate through the network[20–23]. In this mode, the network preferentially transmits temporally precise signals: the firing of neurons in successive layers will either synchronize in the submillisecond range if the input APs are sufficiently correlated, or the firing will fade rapidly[20–23,27]. Under certain conditions, synchrony can be eliminated in the presence of background noise that presumably mimics *in vivo* conditions[4,25]. In this mode, information about input rate, rather than timing, is preferentially propagated through the network. A caveat with these analyses is that the models make simplifying assumptions about the biophysical properties of neurons. The degree to which either temporal or rate coding takes place will likely depend on the filtering characteristics imparted to the neuron by various voltage- and time-dependent conductances.

This study uses an iterative procedure to construct an *in vitro* network of cortical neurons. To examine the coding schemes developed with models, the iteratively constructed network (ICN) was configured to have a feedforward architecture. Although considerably simpler than cortical networks, analyses of feedforward networks have nevertheless provided useful insights into signal propagation. The experiments tests specifically whether input rate can be propagated through the network. To this end, the conditions for the development and elimination of synchrony were examined systematically. The results show that in a simple feedforward network, synchrony developed under a wide range of stimulus conditions and network configurations. Synchrony therefore seems to be the default state. Furthermore, under the conditions of the experiments, synchrony did not encode temporally precise inputs but instead was critically involved in ensuring that rate signals propagated in a stable manner across layers.

RESULTS

Iteratively constructed networks

The ICN consisted of m layers, each consisting of w cells (**Fig. 1a**). The network was sparsely connected: each neuron was innervated by 10% of neurons from the previous layer. Whole-cell recording was established in a pyramidal neuron (in layer 2) using an *in vitro* slice preparation of rat somatosensory cortex[28–31]. This neuron was driven with inputs from a population of simulated layer-1 neurons (filled circles in **Fig. 1a**)[28]. The simulated neurons were made to fire repetitively and asynchronously with respect to each other. Each action potential (AP, **Fig. 1b**) resulted in a postsynaptic current (PSC). A subset (10%) of these neurons was chosen randomly, and their PSC trains were summed. The resultant waveform (**Fig. 1b**, $\mathrm{Sum}_{1,1}$) represented the net synaptic current that the layer-1 neurons' combined activity would generate in a layer-2 neuron. This waveform was then injected under current clamp (unless otherwise stated) into the pyramidal neuron to evoke repetitive firing (**Fig. 1c**, $\mathrm{AP}_{2,1}$). To replicate the activity of another cell (dashed circles) in layer 2, a new current trace ($\mathrm{Sum}_{1,2}$) was calculated and injected into the pyramidal neuron to once again evoke repetitive firing ($\mathrm{AP}_{2,2}$). To complete the first iteration, this process was performed w times, once for each neuron in layer 2. To propagate the signal into the third layer, the procedure was repeated except that simulated layer-1 AP trains were replaced with the evoked 'layer-2' AP trains. When the summed current was injected

Center for Neural Science, New York University, 4 Washington Place, New York, New York 10003, USA. Correspondence should be addressed to A.D.R. (reyes@cns.nyu.edu).

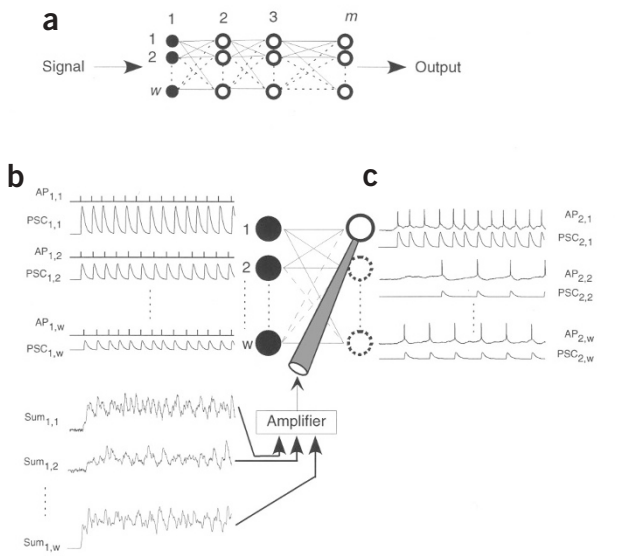

Figure 1 Constructing feedforward networks *in vitro*. (**a**) Networks had *m* layers with *w* neurons per layer. (**b**) The firing (AP) of each neuron in the first layer (●) was simulated, and associated trains of postsynaptic currents (PSCs) were calculated. A randomly chosen subset of PSC trains were summed ($Sum_{1,1}$). (**c**) The summed current was injected into the recorded neuron (which represents a neuron in layer 2) to evoke repetitive action potentials ($AP_{2,1}$). A new summed current trace ($Sum_{1,2}$ in **b**) was then calculated from a different subset of PSC trains and again injected into the neuron. The resultant firing was now equivalent to that of another cell in layer 2 ($AP_{2,2}$). This process was performed *w* times to complete the first iteration. These evoked APs were then used to calculate a new set of PSC trains ($PSC_{2,1}$ to $PSC_{2,w}$). A subset of these trains was again chosen randomly, summed, and the current was re-injected back into the cell. Now, the resultant firing was equivalent to that of a cell in layer 3 (not shown).

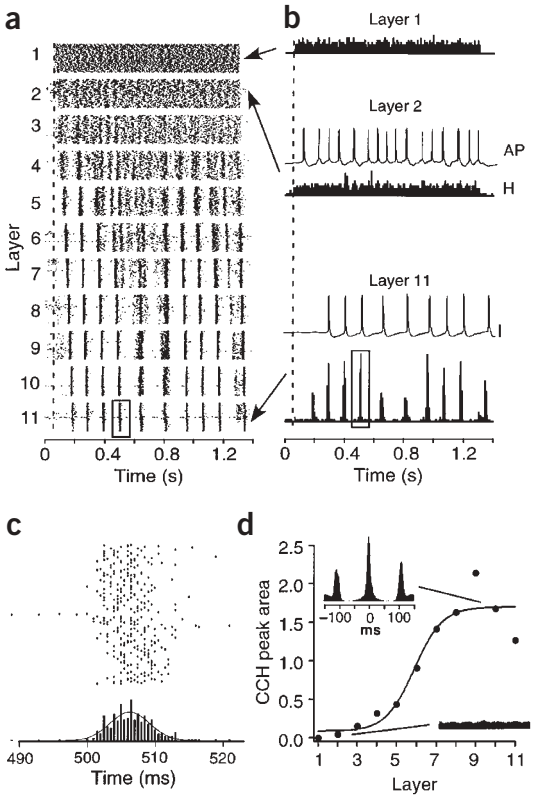

Figure 2 Development of synchrony. (**a**) Dot rasters documenting the firing of neurons in a multi-layer network (200 neurons/layer). Each row of dots represents an action potential (AP) train from a single neuron. (**b**) Time histograms (H) and APs for neurons in selected layers. (**c**) Magnified view of raster and histogram for boxed regions in **a** and **b**. The smooth curve is a Gaussian fit to the histogram. (**d**) Plot of normalized cross-correlation histogram (CCH) peak area versus layer number. Population CCHs (insets) were compiled by cross-correlating the AP trains of all the cells within a layer with each other. Solid curve is the best sigmoid fit. Scale bar in **b**, 20 mV.

into the neuron, the resultant firing was equivalent to that of a cell in the third layer. The pyramidal neuron was once again stimulated *w* times to complete the second iteration. This procedure was iterated *m* times, once for each layer. In this manner, the signal introduced in the first layer could be systematically traced through the network.

The individual PSCs were adjusted so that when injected into a neuron *in vitro*, the resultant voltage deflection was comparable to unitary postsynaptic potentials (PSPs) measured with paired recordings (0.3–1.0 mV)[29,31]. To ensure that the evoked firing (**Fig. 1c**) varied from trial to trial, the amplitudes and latencies of the PSCs were randomized in such a way that the parameters of the associated PSPs were within the range of experimentally measured values[29,31].

Development of synchrony

In every case examined ($n = 60$) under a variety of conditions (see below), neuronal firing was asynchronous for the first 2–3 layers but became progressively more synchronous in successive layers. The occurrences of APs are documented in dot rasters (**Fig. 2a**), where each row of dots represents a train of APs in a given cell, and summarized in population stimulus histograms (H in **Fig. 2b**). In layer 1, the dots in the raster were distributed uniformly and the histogram was flat, confirming that the simulated neurons fired asynchronously with respect to each other. In layer 2, the dots began to cluster, and the histograms began to develop peaks, indicating that the neurons had started to fire synchronously. With each passing layer, the clustering and histogram peaks became sharper to approach a steady level. Magnification of the raster and histogram in layer 11 (boxed regions in **Fig. 2a,b**) shows that the APs within a cluster were distributed normally (**Fig. 2c**). The histogram peak was fitted with a Gaussian function (solid curve), with a standard deviation (s.d.) of 3 ms. To quantify synchrony, cross-correlation histograms (CCHs) were constructed[27,32,33]. The average CCHs (calculated from pairwise correlations of all spike trains in each layer) in the initial layers were flat, whereas those in deeper layers developed peaks that straddle the origin (**Fig. 2d**, insets). The area of the CCH peak above baseline (normalized by the number of sweeps) increased sigmoidally with layer. Note that the peak area in networks with bursting neurons could exceed 1. A sigmoid relation was also obtained with another metric that treated APs in bursts individually[34]. The average (± s.d.) σ of the Gaussian fits to the CCH peaks past layer 5 was 6.0 ± 3.7 ms (range 1.6–13.1; $n = 11$).

Because the input into layer-2 neurons was calculated from a finite ensemble of rhythmically firing layer-1 neurons, the injected current may have had oscillatory temporal structure despite the fact that the layer-1 neurons were uncorrelated. The resultant transients may have provided the seed for synchrony in the second layer. To reduce oscillations, a Poisson process was used to determine the AP times of the layer-1 neurons (**Fig. 3a,b**). In the same network, synchrony developed whether the layer-1 neurons fired in a Poisson or in a repetitive manner (**Fig. 3c**; $n = 5$). Examination of the AP interval distributions

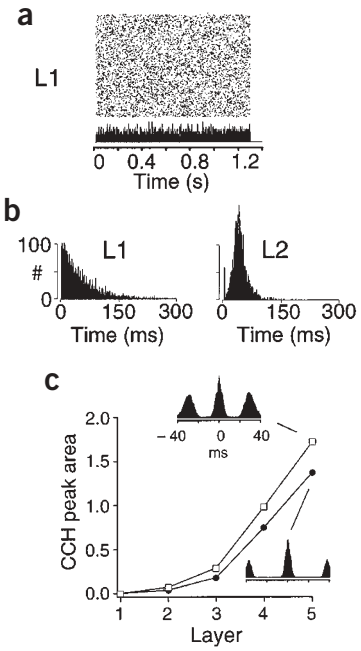

Figure 3 Synchrony with Poisson input. (**a**) Dot rasters of APs in layer 1. The timing of the APs followed a Poisson process (20 Hz). (**b**) Interspike interval distribution of APs in layer 1 (L1) and in layer 2 (L2). (**c**) Plot of normalized CCH peak area versus layer when the layer-1 neurons fired rhythmically (□) and Poissonly (●).

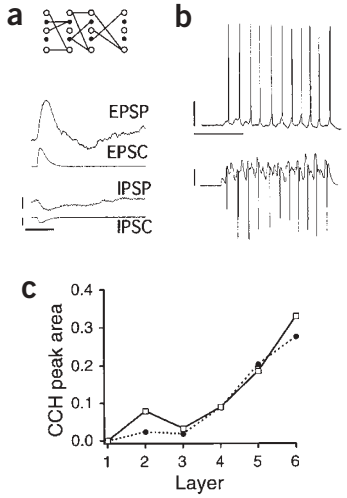

Figure 4 Synchrony in networks with excitatory and inhibitory neurons. (**a**)Voltage (EPSP, IPSP) traces obtained when currents (EPSC, IPSC) were injected under dynamic clamp. The network consisted of an equal number of feedforward excitatory and inhibitory neurons (inset). (**b**) Firing (upper trace) caused by injection of summed current (lower trace). (**c**) Plot of normalized CCH peak area versus layer for networks with only excitatory neurons (140 neurons, □) and for networks with both excitatory and inhibitory neurons (150 each; ●). Vertical scale bars: **a**, 200 V, 0.01 nA; **b**, 20 mV, 0.25 nA. Horizontal scale bars: **a**, 100 ms; **b**, 500 ms.

shows that the firing of neurons in layer 2 did not follow a Poisson process (**Fig. 3b**). In general, the firing of cortical neurons in response to uncorrelated inputs was not Poisson, even in the presence of large background noise (see below).

Synchrony in modified feedforward networks

To determine whether background excitatory and inhibitory inputs reduce synchrony[4], I incorporated feedforward inhibitory neurons into the network (**Fig. 4a**, inset). Excitatory and inhibitory postsynaptic potentials (EPSPs and IPSPs) were evoked in the recorded cell by using a dynamic clamp circuit to inject current (EPSC and IPSC)[35–37] (**Fig. 4a**). Dynamic clamp accurately reproduces the conductance changes caused by synaptic input. The amplitudes of the EPSPs and IPSPs were between 0.3 and 1.0 mV[29–31]. Initially, levels of excitatory and inhibitory inputs were adjusted to be in the 'balanced' configuration so that the mixed input increased the variance but not the mean of the injected current. When injected, the cell's membrane potential fluctuated in the depolarizing and hyperpolarizing directions. One problem was that the recorded neuron fired at very low rates. Unlike in models[4,25,26] and in experiments performed under current-clamp conditions[38,39] where voltage fluctuations frequently cross the threshold for APs, the increase in conductance reduced the voltage excursions to the point where APs were rarely evoked. Increasing the number of inputs had little effect[37]. In practice, a bias toward excitatory inputs was necessary to generate appreciable firing (>10 Hz; **Fig. 4b**) and to prevent the firing rate from fading in successive layers. Under this condition, adding inhibitory neurons to the network did not prevent synchrony ($n = 5$; **Fig. 4c**).

In the models, the tendency toward synchrony may be due to the fact that the network is composed of a single cell type. Because the passive and active properties are the same, the neurons will, on the average, tend to fire at similar times at the stimulus onset (as a result of identical integration times) and thereafter (as a result of identical input/output functions). To determine whether synchrony persists in heterogeneous networks, recordings were made from 2–4 neurons simultaneously. The neurons were chosen so that their input resistances and firing responses were different: some fired repetitively with different degrees of adaptation (**Fig. 5a**), and others fired repetitive bursts (**Figs. 2** and **3**)[40,41]. The neurons were incorporated into the network so that each layer had an equal number of each cell type (**Fig. 5a**, inset). Synchrony still developed after 2–3 layers, whether the network contained two ($n = 5$), three ($n = 4$) or four ($n = 5$) different cells (not shown).

To further increase the firing variability of each neuron, white noise (±0.1 nA) was added to the summed current and injected under current, rather than dynamic, clamp (**Fig. 5b**; $n = 7$). The noise evoked a background firing rate of 10 Hz (which increased to 20 Hz by layer 6) and caused each neuron to fire irregularly (right, distribution of AP intervals). The coefficient of variation of AP intervals was 2.0 in layer 2 and decreased to 1.6 in layer 6. As the dot rasters in layer 6 (**Fig. 5c**) and the plot of CCH peak area (**Fig. 5d**, triangles) show, synchrony was reduced but not eliminated by noise. The effect of higher level noise was not examined because the coefficients of variation of the AP intervals were already at the high end of those commonly reported *in vivo*[4,42,43]. Moreover, the effects of white noise injection may not accurately mimic *in vivo* conditions, particularly if physiological noise arises from uncorrelated inputs[39,42] that generate by a large increase in the neuron's conductance (see above). Synchrony also persisted when: (i) a random steady current bias was introduced from trial to trial to simulate different initial conditions ($n = 3$), (ii) the PSCs showed frequency-dependent changes in amplitudes[30,31,44] ($n = 9$), (iii) the connection probability between neurons was less than 10% (range, 1% to 5%; $n = 5$) or (iv) slow NMDA-like PSCs were used ($n = 6$).

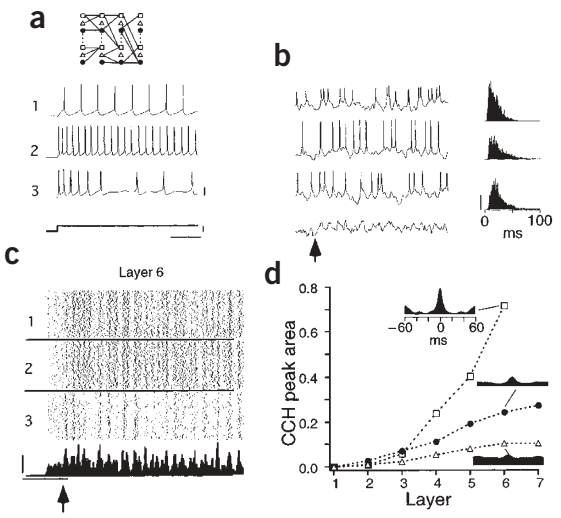

Figure 5 Synchrony in heterogeneous networks. Simultaneous whole-cell recordings were made from three neurons. The neurons were incorporated into the network so that each layer effectively had three cell types (inset). (**a**) Responses of three neurons to current step injection. (**b**) Responses of the same neurons when zero mean white noise current (s.d., ±0.1 nA) was added to the calculated current traces and injected under current clamp. Arrow marks the start of the stimulus. Histograms on right show the distribution of AP intervals. (**c**) Dot rasters of APs in layer 6 in the presence of noise. The network had 240 neurons per layer. Rasters are sorted according to the three cell types. (**d**) Plot of normalized CCH peak area vs. layer for three different levels of white noise current (given as s.d.): □, 0 nA; ●, ±0.05 nA; △, ±0.10 nA. Inset shows CCHs in L6. Vertical scale bars: **a**. 20mV, 0.25 nA; **b**, 50 counts; **c**, 10 counts. Horizontal scale bars in **a** and **c**, 200 ms.

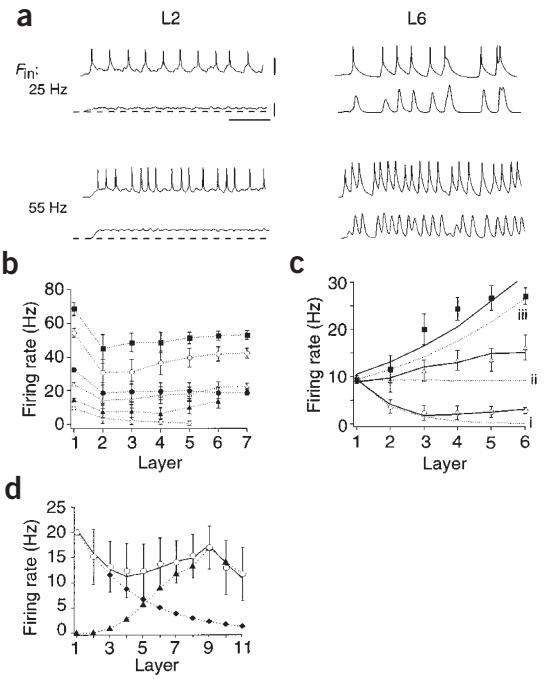

Figure 6 Representation and propagation of frequency signals. (**a**) Action potentials (upper traces) evoked in layer 2 (L2) and layer 6 (L6) neurons when input frequencies of 25 and 55 Hz were delivered to the network. The average current (lower traces) evoked in L2 neurons was steady while that evoked in L6 neurons contained repetitive transients. (**b**) Combined average firing rates (± s.d.) of neurons within a layer plotted against layer (termed the *F–L* curve) for six input frequencies. (**c**) *F–L* curves obtained with 350 (○), 500 (△) and 600 (■) neurons per layer, Superimposed are the predicted asynchronous *F–L* curves (dotted; calculated with $F_{in} = 10$ Hz, $k_1 = 0.02$; $P_w = 0.1$) and the *F–L* curves predicted by a linear combination of synchronous and asynchronous *F–L* curves (solid). Curves in i–iii correspond respectively to cases where the product $k_1{}^*P_w{}^*w$ was less than, equal to, or greater than 1. (**d**) *F–L* curve (○) for the network in **Fig. 2**. Superimposed on the *F–L* curve are the predicted asynchronous (◆) and synchronous (▲) *F–L* curves and the predicted *F–L* curve obtained by their linear sum (solid curve). Vertical scale bars in **a**: 25 mV, 1 nA. Horizontal scale bar: 200 ms.

Synchrony-dependent propagation of input rate

To determine whether the network preserves rate signals, the firing frequency of the each simulated layer-1 neuron (input frequency or F_{in}) was systematically varied ($n = 11$). In all layers, the number of APs that occur during the stimuli increases with F_{in} (**Fig. 6a**, upper traces for both 25 and 55 Hz). The average firing rate of the neurons in each layer, when calculated over the stimulus interval (~1 s) provides information about F_{in}. Plotting the average firing rate (± s.d.) of neurons in a given layer (F) versus layer number (L) gives an '*F–L* curve'. For each of the six input frequencies, the *F–L* curves reached a steady level by layers 2–4 and were distinguishable from each other (**Fig. 6b**).

The changes in firing rates in the initial and deeper layers occurred through different mechanisms[28,45,46]. In layer 2, asynchronous inputs generated a predominantly steady current that caused the neuron to fire repetitively (**Fig. 6a**, lower traces). In this regime, the firing rate varied with the magnitude of the average current, which in turn varied with input frequency[28]. In layer 6, synchronous inputs generated suprathreshold current transients that occurred repetitively. In this regime, the firing rate was determined by the frequency of the transients. The responses of neurons to asynchronous (or steady current) and synchronous (or transient current pulses) inputs differ even when the input rates (or average current) are identical[28,46].

Without synchrony, rate signals would propagate in an unstable manner across layers. This can be seen by calculating the *F–L* curves that would be obtained if synchrony had not developed in the network. In this hypothetical scenario, the firing of neurons within a given layer depends only on the rate of arrival of inputs. The firing rate (F_{as}) evoked by asynchronous input can be approximated in the unsaturated firing regime by

$$F_{as} = k_1{}^*F_{pre}{}^*N_{pre} = k_1{}^*F_{pre}{}^*P_w{}^*w \quad (1)$$

where k_1 is a constant determined experimentally[28], F_{pre} and N_{pre} are the firing rate and number of presynaptic neurons, and P_w is the connection probability of neurons between layers. The term $P_w{}^*F_{pre}{}^*w$ gives the arrival rate of inputs. Because $P_w{}^*w$ is constant, the firing rate of neurons in the successive layers can be calculated by using equation (1) iteratively:

$$F_{as(L)} = k_1{}^*P_w{}^*w{}^*F_{as(L-1)} = (k_1{}^*P_w{}^*w)^{L-1}{}^*F_{in} \quad (2)$$

The predicted asynchronous *F–L* curves decreased when $k_1{}^*P_w{}^*w < 1$ (**Fig. 6c**, curve i) and increased when $k_1{}^*P_w{}^*w > 1$ (curve iii); only when $k_1{}^*P_w{}^*w = 1$ (curve ii) did the *F–L* curves remain stable. The experimental *F–L* curves, on the other hand, reached steady-state by layer 4 (**Fig. 6c**). In general, the asynchronous *F–L* curves matched the experimentally measured *F–L* curve only for the first 2–4 layers.

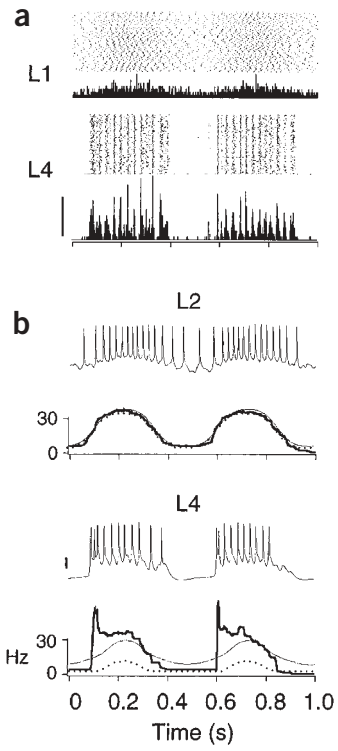

Figure 7 Synchrony with sinusoidally modulated inputs. (**a**) Dot rasters and histograms of APs in layers 1 and 4. The firing rates of neurons in layer 1 were sinusoidally modulated at 2 Hz with peak/trough values of 45/15 Hz. (**b**) APs (first and third traces) and instantaneous firing rates (second and fourth traces) of neurons in layers 2 and 4. The firing rates predicted from only the asynchronous component (dotted traces) and from the sum of asynchronous and synchronous components (thin traces) are superimposed on the experimentally measured firing rate (thick traces). Vertical scale bar in **a**, 25 counts; **b**, 20 mV.

Synchrony had a crucial role in propagating signals in the deeper layers. The change in overall firing rate contributed by synchrony (F_s) can be described by $F_{s(L)} = k_2{}^*F_{in}{}^*A_L$, where A is the normalized CCH peak area. For the network in **Fig. 6d**, the value of $k_2{}^*F_{in}$ was approximated by dividing the firing rate in layer 11 (circles) by the corresponding CCH area (**Fig. 2d**). By layer 11, the contribution of F_{as} (**Fig. 6d**, diamonds) to the overall firing rate is nearly zero. The synchronous *F–L* curve (triangles) complemented the asynchronous *F–L* curve in that it matched the experimental *F–L* curve only past layer 6. This suggests that firing rate depends on asynchrony in the initial layers but then on synchrony in the deeper layers.

The experimental *F–L* curve was predicted by linearly combining the asynchronous and synchronous *F–L* curves (**Fig. 6d**, solid curve):

$$F_{pred(L)} = a^*F_{as(L)} + b^*F_{s(L)} \quad (3)$$

The coefficients a and b were determined using a least squares fit. The predicted *F–L* curves were accurate when the asynchronous *F–L* curve decayed to zero or remained constant ($k_1{}^*P_w{}^*w \leq 1$); they were less accurate when $k_1{}^*P_w{}^*w > 1$ because the asynchronous *F–L* curve continued to increase while both the experimental and synchronous *F–L* curves plateaued (**Fig. 6c**). A better fit might be obtained if the linear input/output relation in equation (1) is replaced with a sigmoid function.

To determine whether synchrony-based coding of rate can be generalized to time-varying signals, a sinusoidally modulated F_{in} was delivered to the network (**Fig. 7**; $n = 5$). As was the case for constant F_{in}, neurons started to fire synchronously by layer 3 or 4. Neuronal firing, depicted as the instantaneous firing rate averaged over all neurons within a layer, remained modulated in successive layers (**Fig. 7b**, thick lines). The firing rate of neurons in layer 2 varied sinusoidally; however, those of neurons in deeper layers were somewhat distorted, suggesting that synchrony-based rate coding may be better suited for constant or slowly modulated input frequencies.

As with constant F_{in}, the firing response to time-varying F_{in} can be described as a sum of an asynchronous and a synchronous term (Methods). The predicted asynchrony-based firing rate for the sinusoidal input (dotted lines in **Fig. 7b**) accurately described firing in layer 2 but underestimated firing in layer 4 and was nearly zero by layer 6 (not shown). Adding a term proportional to the level of synchrony improved the predicted firing curve substantially (thin line) though the curve failed to describe the transient bursts. Nevertheless, these analyses indicate that without synchrony, time-varying rate signals do not propagate.

DISCUSSION

Comparison with synchrony in models

In the ICN, as in the models[20–23,27], the firing of neurons in successive layers either synchronized or degraded to zero. Theoretical analyses suggest that synchrony develops when a sufficiently large number of input spikes occur within a time interval ('spike packets'). A similar condition likely applies to the ICN, albeit with input spikes that are distributed uniformly rather than normally. Unlike in models, synchrony in the ICN was beyond the submillisecond range. Temporal precision was reduced by the variable PSC latencies incorporated into the ICN, by the tendency of some neurons to burst, and by the presence of a 'soft' threshold in cortical neurons that causes APs to occur at variable delays after an EPSP[45]. Another difference is that synchrony in the ICN was resistant to background noise. In integrate-and-fire neurons, unlike in cortical neurons[45], the membrane trajectory in the interspike interval rises exponentially and spends more time hovering near threshold. Consequently, relatively smaller voltage fluctuations can cross threshold and disrupt AP timing. The impact of noise may be further reduced by the fact that the combined properties of voltage- and time-dependent conductances in cortical neurons enhance the effectiveness of large, transient inputs (**Fig. 6a**) for evoking APs[28,38,42,46,47].

In these experiments, synchrony did not convey coincident events because the input signals were uncorrelated. Rather, synchrony had an important, albeit permissive, role in propagating rate signals: it ensured that the repetitive current transients in successive layers (**Fig. 6a**) were sufficiently large to evoke APs. Computing rate with the synchrony-based code requires a time window of at least one interspike interval. For example, to discriminate frequency inputs above 20 Hz, a time window of at least 50 ms is needed. This relatively long time window suggests that the synchrony-based coding of rate may apply more to long-lasting events such as the coherent oscillations that appear in cortex during specific motor-related tasks[13–16]. However, if the functionally relevant range of firing rates is high, the time window may not be grossly different from that needed for 'fast' propagation of rate signals via an asynchrony-based code[25]. In neurons of the visual cortex, the APs evoked with sine-wave grating stimuli are due to large, synchrony-mediated voltage transients that occur in the γ frequency range[48,49].

Comparison with synchrony *in vivo*

Overall, the level of synchrony in the ICN was higher than *in vivo*[16,33,50]. This discrepancy probably did not result from the use of a fixed and finite ensemble of AP trains to construct network activity, as cortical neurons also receive a finite number of inputs. That cortical networks are more complex and therefore generate more noise also cannot explain the difference. Because voltage fluctuations are limited by conductance increases that accompany synaptic input, it seems unlikely that presence of feedback circuits would generate more variability than noise injected under current clamp (**Fig. 5**). A possible explanation is that neurons belonging to a particular network *in vivo* may multiplex several synchronous signals from other networks. Any differences in the sets of input signals to each neuron would decrease synchrony within that network. Indeed, synchronous barrages may underlie the large firing variability observed *in vivo*[39,42].

At first glance, the high level of synchrony in the ICN seems to be more symptomatic of epileptiform activity. However, given that the minimum number of neurons needed to propagate signals (100–300 neurons per layer with $P_w = 0.1$) is only a small fraction of cortical neurons, full-scale epileptiform activity need not develop throughout cortex during normal activity.

METHODS

Surgical procedures. Surgical, slicing and recording techniques were done as described previously[28–31] and followed guidelines established by the NYU Animal Welfare Committee. Slices were made from the sensorimotor cortex of Wistar rats (21 days or older). During recordings, slices were perfused with artificial cerebrospinal fluid (125 mM NaCl, 2.5 mM KCl, 25 mM glucose, 25 mM $NaHCO_3$, 1.25 mM NaH_2PO_4, 2 mM $CaCl_2$ and 1 mM $MgCl_2$) heated to 31–34 °C. Layer-5 pyramidal neurons were identified under infrared differential interference contrast videomicroscopy. Whole-cell recordings were performed with pipettes with d.c. resistances of 5–10 MΩ when filled with 100 mM potassium gluconate, 20 mM KCl, 4 mM MgATP, 10 mM phosphocreatine, 0.3 mM GTP and 10 mM HEPES). Voltage and current signals were filtered at 10 kHz and digitized at 2–10 kHz.

Stimulation protocol. A computer program simulated the activities of a specified number of presynaptic cells. Each simulated cell fired repetitively for 1 s at a specified average rate (AP, **Fig. 1b**). To ensure that the neurons' firing were not temporally correlated the following procedures were used: (i) jitter was added to the interspike intervals (ISIs) such that the ISIs were distributed normally about a mean interval with a standard deviation of ±10% of the ISI; (ii) the start times of the spike trains were uniformly distributed within one ISI. Each time a simulated cell fired an AP, an associated synaptic current (PSC) was calculated. The time course of the current was described by $PSC(t) = k_{amp}(1 - e^{-t/\tau 0})e^{-t/\tau 1}$ where k_{amp} is the amplitude, and τ_0 (1 ms) and τ_1 (2 ms) are time constants. The individual PSCs were adjusted so that when injected into a neuron *in vitro*, the resultant voltage deflection was comparable to unitary postsynaptic potentials (PSPs) measured with paired recordings[29–31]. The PSCs were convolved with the spike trains of each presynaptic cell.

Each injected current trace (for example, $Sum_{1,1}$ and $Sum_{1,2}$) was calculated by randomly choosing and then summing a subset (1–10%) of PSC trains at each layer. The current trace was converted to an analog signal and injected into the cell via the amplifier and recording electrode. The amplitudes (mean ± s.d., 1.0 ± 0.9 mV) and latencies (1.7 ± 0.9 ms) of the PSPs were randomized in each trial. The number of neurons per layer was adjusted so that when the summed PSCs were injected, the firing rate of the recorded neuron was equal to that of the simulated neuron. This ensured that the signal was propagated successfully from layer to layer. Stimuli were delivered at intervals of ≥3 s.

For experiments with dynamic clamp, two patch electrodes, one for recording membrane potential and the other for injecting current, were placed at the soma[37]. An analog dynamic circuit injected current that was proportional to the membrane potential (V): $PSC(t) = g(t)^*(V - E_{rev})$ where $g(t)$ is the computer-generated conductance change, and E_{rev} is the reversal potential for excitatory (0 mV) or inhibitory (–80 mV) PSCs. The AP trains of the simulated and recorded neurons were used to generate a set of both excitatory and inhibitory conductance trains. The two sets of trains were converted to analog signals and routed through separate channels in the dynamic clamp circuit. The circuit converted the conductance waveforms to EPSC and IPSC trains and then summed them before injection into the neuron.

Prediction of temporally modulated firing. The predicted asynchrony- and synchrony-based firing rates ($F_{as}(t)$ and $F_s(t)$; **Fig. 7**) in response to sinusoidal F_{in} were calculated as follows. The constants in equations (1–3) were first determined by delivering a constant F_{in} to the network. To calculate $F_{as}(t)$, the instantaneous firing rates of the simulated layer-1 and recorded layer-2 neurons were calculated, averaged and plotted against each other for each time point ($F_{as}(t)_2$ versus $F_{as}(t)_1$). The sigmoid fit to the data gives the input/output function ($F_{as2} = S(F_{as1})$ of the neuron. This equation was iteratively applied to determine the firing rate across layers: $F_{as}(t)_L = S(F_{as}(t)_{L-1})$. Note that equation (1) can also be used to calculate $F_{as}(t)_L$. The synchrony-based component is given by: $F_s(t)_L = k_2{}^*A_L{}^*F_1(t)$ where the coefficient k_2 was determined in layer 6 (where $F_{as}(t)$ is zero) by curve fitting and A is the corresponding CCH peak area. Summing $F_{as}(t)$ and $F_s(t)$ gives the predicted firing rate in successive layers (**Fig. 7**, thin line).

ACKNOWLEDGMENTS

The author wishes to thank H. Cateau, F. Chance, T. Lewis and R. Shapley for providing helpful comments. This work was supported by National Science Foundation grant IBN–0079619 and by the Edith J. Low-Beer foundation.

COMPETING INTERESTS STATEMENT

The author declares that he has no competing financial interests.

Received 11 March; accepted 9 April 2003
Published online 5 May 2003; doi:10.1038/nn1056

1. Abeles, M. *Corticonics* 208–258 (Cambridge Univ. Press, Cambridge, 1991).
2. Shadlen, M.N. & Newsome, W.T. Noise, neural codes and cortical organization. *Curr. Opin. Neurobiol.* **4**, 569–579 (1994).
3. Ferster, D. & Spruston, N. Cracking the neuronal code. *Science* **270**, 756–757 (1995).
4. Shadlen, M.N. & Newsome, W.T. The variable discharge of cortical neurons: implications for connectivity, computation and information coding. *J. Neurosci.* **18**, 3870–3896 (1998).
5. Shadlen, M.N. & Movshon, J.A. Synchrony unbound: a critical evaluation of the temporal binding hypothesis. *Neuron* **24**, 67–77 (1999).
6. Meister, M. & Berry, M.J. The neural code of the retina. *Neuron* **22**, 435–450 (1999).
7. Borst, A. & Theunissen, F.E. Information theory and neural coding. *Nat. Neurosci.* **2**, 947–957 (1999).
8. deCharms, R.C. & Zador, A. Neural representation and the cortical code. *Annu. Rev. Neurosci.* **23**, 613–647 (2000).
9. Van Rullen, R. & Thorpe, S.J. Rate coding versus temporal order coding: what the retinal ganglion cells tell the visual cortex. *Neural Comp.* **13**, 1255–1283 (2001).
10. Riehle, A., Grun, S., Diesmann, M. & Aertsen, A. Spike synchronization and rate modulation differentially involved in motor cortical function. *Science* **278**, 1950–1953 (1997).
11. Prut, Y. *et al.* Spatiotemporal structure of cortical activity: properties and behavioral relevance. *J. Neurophysiol.* **79**, 2857–2874 (1998).
12. Hatsopoulos, N.G., Ojakangas, C.L., Paninksi, L. & Donoghue, J.P. Information about movement direction obtained from synchronous activity of motor cortical neurons. *Proc. Natl. Acad. Sci. USA* **95**, 15706–15711 (1998).
13. Murthy, V.N. & Fetz, E.E. Coherent 25–35 Hz oscillations in the sensorimotor cortex of awake behaving monkeys. *Proc. Natl. Acad. Sci. USA* **89**, 5670–5674 (1992).
14. Baker, S.N., Kilner, J.M., Pinches, E.M. & Lemon, R.N. The role of synchrony and oscillations in the motor output. *Exp. Brain Res.* **128**, 109–117 (1999).
15. Conway, B.A. *et al.*, Synchronization between motor cortex and spinal motoneuronal pool during the performance of a maintained motor task in man. *J. Physiol.* **489**, 917–924 (1995).
16. Baker, S.N., Spinks, R., Jackson A. & Lemon, R.N. Synchronization in monkey motor cortex during a precision grip task. I. Task–dependent modulation in single–unit synchrony. *J. Neurophysiol.* **85**, 869–885 (2001).
17. Feige, B., Aertsen, A. & Kristeva–Feige, R. Dynamic synchronization between multiple cortical motor areas and muscle activity in phasic voluntary movements. *J. Neurophysiol.* **84**, 2622–2629 (2000).
18. Panzeri, S., Petersen, R.S., Schultz, S.R. & Lebedev, M. The role of spike timing in the coding of stimulus location in rat somatosensory cortex. *Neuron*, **29**, 769–777 (2001).
19. Abeles, M., Bergman, E., Margalit, H. & Vaadia, E. Spatiotemporal firing patterns in the frontal cortex of behaving monkeys. *J. Neurophysiol.* **70**, 1629–1638 (1993).

20. Diesmann, M., Gewaltig, M.O. & Aertsen, A. Stable propagation of synchronous spiking in cortical neural networks. *Nature* **402**, 529–533 (1999).
21. Cateau, H. & Fukai, T. Fokker–Planck approach to the pulse packet propagation in synfire chain. *Neural Net.* **14**, 675–685 (2001).
22. Diesmann, M., Gewaltig, M., Rotter, S. & Aertsen, A., State space analysis of synchronous spiking in cortical neural networks. *Neurocomputing* **565**, 38–40 (2001).
23. Gewaltig M., Diesmann, M. & Aertsen A. Propagation of cortical synfire activity: survival probability in single trials and stability in the mean. *Neural Net.* **14**, 657–673 (2001).
24. Barlow, H.B. Single units and sensation: a neuron doctrine for perceptual psychology? *Perception* **1**, 371–394 (1972).
25. van Rossum, M.C., Turrigiano, G.G. & Nelson, S.B. Fast propagation of firing rates through layered networks of noisy neurons. *J. Neurosci.* **22**, 1956–1966 (2002).
26. Mazurek, M.E. & Shadlen, M.N. Limits to the temporal fidelity of cortical spike rate signals. *Nat. Neurosci.* **5**, 463–471 (2002).
27. Litvak, V., Sompolinsky, H., Segev, I. & Abeles, M. On the transmission of rate code in long feed-forward networks with excitatory–inhibitory balance. *J. Neurosci.* **23**, 3006–3015 (2003).
28. Oviedo, H. & Reyes, A.D. Boosting of neuronal firing evoked with asynchronous and synchronous inputs to the dendrite. *Nat. Neurosci.* **5**, 261–266 (2002).
29. Markram, H., Lubke, J., Frotscher, M., Roth, A. & Sakmann, B. Physiology and anatomy of synaptic connections between thick tufted pyramidal neurons in the developing rat neocortex. *J. Physiol.* **500**, 409–440 (1997).
30. Reyes, A.D. *et al.* Target-cell–specific facilitation and depression in neocortical circuits. *Nat. Neurosci.* **1**, 279–285 (1998).
31. Reyes, A.D. & Sakmann, B. Developmental switch in the short-term modification of unitary EPSPs evoked in layer 2/3 and layer 5 pyramidal neurons of rat neocortex. *J. Neurosci.* **19**, 3827–3835 (1999).
32. Perkel, D.H., Gerstein, G.L. & Moore, G.P. Neuronal spike trains and stochastic point processes. II. Simultaneous spike trains. *Biophys. J.* **7**, 419–440 (1967).
33. Fetz, E., Toyama, K. & Smith, W. Synaptic interactions between cortical neurons. *Cereb. Cortex* **9**, 1 (1991).
34. Pinsky, P.F. & Rinzel, J. Synchrony measures for biological neural networks. *Biol. Cybern.* **73**, 129–37 (1995).
35. Sharp, A., O'Neil, M.B., Abbott, L.F. & Marder, E. The dynamic clamp: artificial conductances in biological neurons. *TINS* **16**, 389–394 (1993).
36. Reyes, A.D., Rubel, E.W. & Spain, W.J. *In vitro* analysis of optimal stimuli for phase-locking and time-delayed modulation of firing in avian nucleus laminaris neurons. *J. Neurosci.* **16**, 993–1007 (1996).
37. Chance, F., Abbott, L.F. & Reyes, A.D. Gain modulation from background synaptic input. *Neuron* **35**, 773–782 (2002).
38. Mainen, Z.F. & Sejnowski, T.J. Reliability of spike timing in neocortical neurons. *Science* **268**, 1503–1506 (1995).
39. Stevens, C.F. & Zador, A. Input synchrony and the irregular firing of cortical neurons. *Nat. Neurosci.* **1**, 210–217 (1998).
40. Connors, B.W. & Gutnick, M.J. Intrinsic firing patterns of diverse neocortical neurons. *Trends Neurosci.* **13**, 99–104 (1990).
41. Schwindt, P.C., O'Brien, J.A. & Crill, W.E. Quantitative analysis of firing properties of pyramidal neurons from layer 5 of rat sensorimotor cortex. *J. Neurophysiol.* **77**, 2484–2498 (1997).
42. Softky, W. & Koch, C. The highly irregular firing of cortical cells is inconsistent with temporal integration of random EPSPs. *J. Neurosci.* **13**, 334–350 (1993).
43. Holt, G.R., Softky, W.R., Koch, C. & Douglas, R.J. Comparison of discharge variability *in vitro* and *in vivo* in cat visual cortex neurons. *J. Neurophysiol.* **75,** 1806–1814 (1996).
44. Markram, H., Wang, Y. & Tsodyks, M. Differential signaling via the same axon of neocortical pyramidal neurons. *Proc. Natl. Acad. Sci. USA* **9**, 5323–5328 (1998).
45. Reyes, A.D. & Fetz, E.E. Effects of transient depolarizing potentials on the firing rate of cat neocortical neurons. *J. Neurophysiol.* **69**, 1673–1682 (1993).
46. Reyes, A.D. & Fetz, E.E. Two modes of interspike interval shortening by brief transient depolarizations in cat neocortical neurons. *J. Neurophysiol.* **69**, 1661–1672 (1993).
47. Baker, S.N. Quantification of the relative efficacies of asynchronous and oscillating inputs to a motoneuron pool using a computer model. *J. Physiol.* **504**, 116 (1997).
48. Azouz, R. & Gray, C.M. Cellular mechanisms contributing to response variability of cortical neurons *in vivo*. *J. Neurosci.* **19**, 2209–2223 (1999).
49. Azouz, R. & Gray, C.M. Adaptive coincidence detection and dynamic gain control in visual cortical neurons *in vivo*. *Neuron* **37**, 513–523 (2003).
50. Matsumura, M. *et al.* Synaptic interactions between primate precentral cortex neurons revealed by spike–triggered averaging of intracellular membrane potentials *in vivo*. *J. Neurosci.* **16**, 7757–7767 (1996).